ADVANCED MATERIALS INTERFACES
Open Access
www.advmatinterfaces.de

Supramolecular Nanoarchitectonics of PNIPAAM-co-MA and Imogolite to Obtain Thermoresponsive Clay Nanotubes Through Complexation Mechanism

Claire Hotton, Lorenzo Lisuzzo, Giuseppe Cavallaro, Erwan Paineau,* Thomas Bizien, and Giuseppe Lazzara*

In this study, the colloidal properties of hybrids formed by imogolite nanotubes (INTs) and poly(*N*-isopropylacrylamide)-co-methacrylic (PNIPAAM-co-MA) are investigated, which is a thermo-sensitive copolymer suitable for drug delivery applications. The selective adsorption of anionic PNIPAAM-co-MA onto the positively charged external surface of imogolite is driven by electrostatic attractions as evidenced by both ζ-potential and Dynamic Light Scattering (DLS) experiments. According to polarized optical observations and Small-angle X-ray scattering (SAXS) measurements, the specific interactions with PNIPAAM-co-MA affect the structural organization of imogolite nanotubes, destabilizing the nematic phase. On the other hand, the formation of PNIPAAM-co-MA/INTs complex alters the thermo-responsive characteristics of the copolymer due to variations on the thermodynamics of the coil-to-globule transition of PNIPAAM-co-MA. Thermodynamic characterizations (Differential Scanning Calorimetry, Density and Speed of sound experiments) reveal that the lower crystalline solution temperature (LCST) of PNIPAAM-co-MA is reduced in the presence of imogolite nanotubes. The attained knowledge represents a starting point to develop thermo-responsive clay nanotubes useful for biomedical purposes by exploiting the selective coating of imogolite with PNIPAAM-co-MA.

1. Introduction

The combination of functional polymers and inorganic nanoparticles has been recently investigated to develop advanced materials useful for numerous applications, including biomedicine,[1–7] catalysis,[8–10] remediation,[11–14] and packaging.[15–17] The morphological characteristics of the nanoparticles are crucial to determine the properties and the functionalities of the composite materials.[18–24] In this regard, nanomaterials with a hollow tubular shape can be suitable for different purposes due to their cavity, which can be exploited for the confinement of chemically and biologically active molecules.[25–28] Among nanotubes, imogolite clay is an emerging particle because of its structure and surface properties (**Scheme 1**).[22,29–32] The size of imogolite nanotubes (INTs) depends on their synthesis procedure.[33,34] Single-walled imogolite nanotubes exhibit an average outer diameter of 2.5 nm, while the inner diameter range between 1.5 and 2.0 nm.[33] The nanotube length is from 100 nm to a few micrometers.[29] Aluminogermanate double-walled imogolite presents a larger external diameter (≈4.5 nm) with an aspect ratio that can be tuned in a wide range (from 6 to 210).[35,36] Literature reports that the aspect ratio of imogolite affects the self-assembling mechanisms of the nanotubes dispersed in aqueous solvents because of excluded volume interactions.[37,38] Although their low concentration, imogolite dispersions can generate liquid crystalline phases due to repulsive interactions between INTs.[39] Interestingly, the inner and outer surfaces of imogolite possess different chemical composition and, consequently, opposite charges in a large pH interval.[40] The inner surface is formed by silanol groups (≡Si—OH), whereas aluminol groups (≡Al—OH and ≡Al_2—OH) are predominant on the INTs shell. Below the INTs isoelectric point (pH 10.5), the outer surface is positively charged (Scheme 1), allowing to the selective adsorption of anionic molecules in agreement to electrostatic attractions as demonstrated for DNA[41] and sacran polysaccharide.[42] Oppositely, the negative charges of inner surface could lead

C. Hotton, E. Paineau
Université Paris-Saclay
CNRS
Laboratoire de Physique des Solides
Orsay 91405, France
E-mail: erwan-nicolas.paineau-lanone@cnrs.fr
L. Lisuzzo, G. Cavallaro, G. Lazzara
Department of Physics and Chemistry "Emilio Segrè"
University of Palermo
Viale delle Scienze 17, Palermo 90128, Italy
E-mail: giuseppe.cavallaro@unipa.it
T. Bizien
Synchrotron SOLEIL
L'Orme des Merisiers
91192 Gif-sur-Yvette Cedex, France

The ORCID identification number(s) for the author(s) of this article can be found under https://doi.org/10.1002/admi.202500211

DOI: 10.1002/admi.202500211

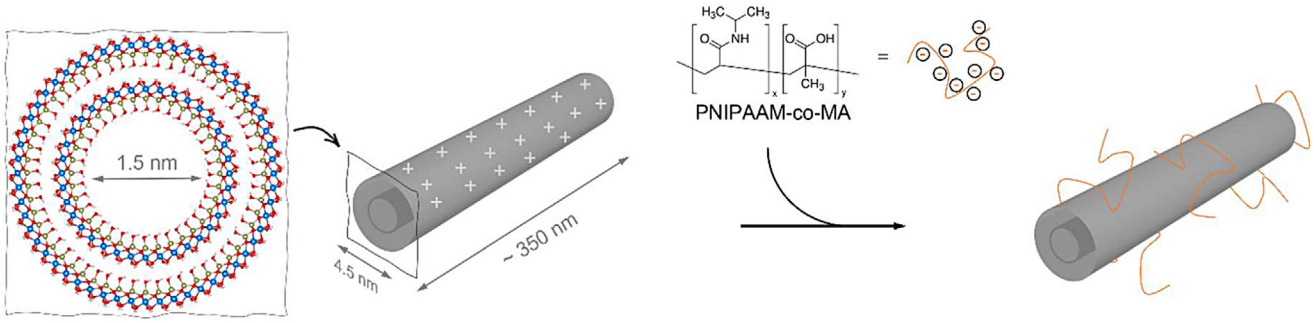

Scheme 1. Illustration of the structure of the as-synthesized double-walled aluminogermanate nanotubes and its functionalization by direct blending with an anionic polymer, poly(*N*-isopropylacrylamide)-co-methacrylic acid (PNIPAAM-co-MA). Al, Ge, O, and H atoms are shown in blue, gold, red, and white, respectively.

to the encapsulation of cationic molecules inside the INTs cavity.

Here, we studied aqueous mixtures of INTs and poly(*N*-isopropylacrylamide)-co-methacrylic acid (PNIPAAM-co-MA), which is an anionic polymer with thermosensitive properties. As shown in Scheme 1, the electrostatic attractions between anionic PNIPAAM-co-MA and INTs outer surface (positively charged) can lead to the coating of clay nanotubes with thermosensitive polymeric chains. According to literature,[43–45] PNIPAAM based polymers can be employed as gels and nanocarriers for drug delivery applications useful in pharmaceutics and biomedicine. Poly(*N*-isopropylacrylamide) shows a coil-to-globule transition at ≈32 °C, which represents the low critical solution temperature (LCST) of the polymer. The structural variation of PNIPAAM from hydrophilic coil to hydrophobic globule can be exploited for the controlled release of drugs under temperature stimuli, which might simulate specific physiological conditions. Copolymerization of PNIPAAM with both hydrophilic and hydrophobic molecules can alter the LCST allowing to tune the properties of the polymer for specific applications.[46–48] The modification of PNIPAAM by ionic molecules drives to obtain thermosensitive and charged polymers. Negatively charged PNIPAAMs are synthesized by the addition of carboxylic termination as well as by copolymerization with methacrylic acid.[48–50] On the other hand, the introduction of amine groups to PNIPAAM leads to synthesizing a cationic macromolecule.[48] PNIPAAMs modified with ionic groups were used for selective functionalization of inorganic nanoparticles through both covalent and supramolecular interactions, allowing to obtaining of hybrid materials with thermo-responsive behavior.[48,51–53]

This work reports an extensive characterization of INTs/PNIPAAM-co-MA aqueous mixtures from electrostatic, structural, and thermodynamic viewpoints. The findings demonstrate that the coating of imogolite with PNIPAAM-co-MA is suitable for developing thermo-responsive nanotubes promising as drug delivery systems. Similarly to small molecule-based systems,[54,55] metal supramolecular assemblies[56,57] and clay-based organic inorganic composite materials,[58] thermo-sensitive INTs/PNIPAAM-co-MA hybrids might be suitable for applications in smart windows and soft actuating devices.

2. Results and Discussion

2.1. Adsorption of PNIPAAM-co-MA onto Imogolite Nanotubes

The synthesis of aluminogermanate double-walled nanotubes was realized in a single-step process under hydrothermal conditions under autogenous pressure as described in the Experimental Section. The characterization by transmission electron microscopy and infrared spectroscopy confirms the successful synthesis of INTs (see Figure S1, Supporting Information) in agreement with our previous reports.[59,60] The functionalization of imogolite with PNIPAAM-co-MA was demonstrated by studying the effects of polymer addition on the surface charge and aqueous dynamic behavior of clay nanotubes as illustrated in Scheme 1. Moreover, polarized optical observations and SAXS experiments evidenced that PNIPAAM-co-MA affects the structural organization of imogolite, confirming the polymer adsorption onto nanoclays.

2.1.1. Surface Charge and Aqueous Dynamic Behavior of Imogolite/PNIPAAM-co-MA Complexes

Figure 1A compares the ζ-potential data of imogolite nanotubes before and after the addition of variable PNIPAAM-co-MA amounts.

According to their surface chemical composition, pristine INTs are positively charged as evidenced by their ζ-potential value (+29 ± 2 mV), which agrees with literature data.[35,61] Imogolite can interact by electrostatic attractions with PNIPAAM-co-MA, which possesses a negative surface charge due to the presence of methacrylic acid.[48] Specifically, we calculated a ζ-potential value of −10.4 ± 1.2 mV for neat PNIPAAM-co-MA. As shown in Figure 1A, PNIPAAM-co-MA addition induced an inversion of the INTs ζ-potential that can be attributed to the neutralization of the positive charges of imogolite outer surface, which is formed by Al-OH groups. Namely, ζ-potential results reflect the selective adsorption of the anionic copolymer onto the positive INTs shell. Accordingly, it is reported that the selective functionalization of imogolite external surface can reached by exploiting electrostatic attractions with anionic species, such as selenate,[62] perchlorates,[63] and aminoacids.[64] Recently, Hotton et al.

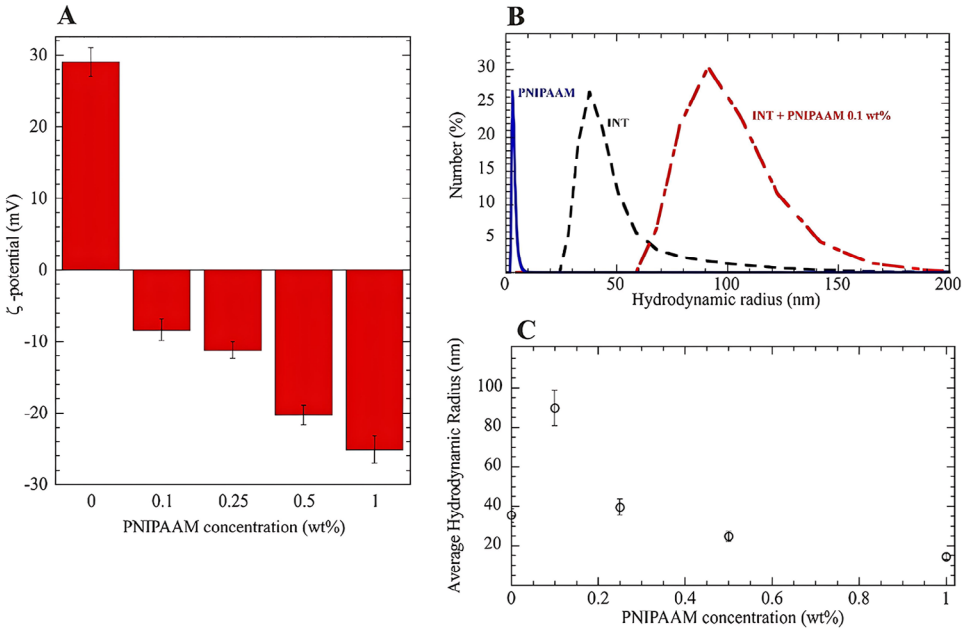

Figure 1. Surface charge and aqueous diffusion of imogolite/PNIPAAM-co-MA. A) ζ-potential of imogolite nanotubes as a function of PNIPAAM-co-MA concentration. B) Number-weighted distributions obtained from DLS measurements for hydrodynamic radii of aqueous dispersions of PNIPAAM-co-MA, imogolite and imogolite/PNIPAAM-co-MA. The concentrations of imogolite and polymer are 0.01 and 0.1 wt.%, respectively. C) Average hydrodynamic radius for imogolite/PNIPAAM-co-MA hybrids with variable polymer concentrations.

investigated the colloidal behavior of INT in symmetric (NaCl) and asymmetric electrolytes (Na_2SO_4 and Na_3PO_4).[60] On the other hand, it was proved that PNIPAAM-co-MA is successful in the selective modification of halloysite inner surface, which is composed by alumina groups.[48]

Moreover, we observed that the influence of PNIPAAM-co-MA adsorption onto the ζ-potential of imogolite is proportional to the copolymer concentration within the investigated range (0.1–1 wt.%). As expected, the increase of PNIPAAM-co-MA content favors the neutralization of INTs aluminol groups highlighting that the copolymer saturation of imogolite surface was not reached.

The adsorption process was demonstrated also by studying the effects of PNIPAAM-co-MA on the aqueous dynamic behavior of imogolite nanotubes through Dynamic Light Scattering (DLS).

As a general result, the field-time autocorrelation curves of imogolite and PNIPAAM-co-MA aqueous dispersions as well as INTs/PNIPAAM-co-MA aqueous mixtures can be described by monoexponentially functions. The latter highlights that the copolymer adsorption does not alter the single-diffusive characteristic of imogolite nanotubes. The fitting analysis of autocorrelation curves by ILT (Inverse Laplace Transform) allowed us to determine the distributions of the hydrodynamic radii (Figure 1B). According to literature,[48] the distribution of pristine PNIPAAM-co-MA range between 2 and 3 nm. The addition of 0.1 wt.% PNIPAAM-co-MA significantly shifted the distribution of the INTs hydrodynamic radii to larger values indicating that the copolymer adsorption reduced the aqueous mobility of imogolite nanotubes. This effect can be related to the alteration of the INTs surface charge generated by PNIPAAM-co-MA. As compared with pristine imogolite, the presence of 0.1 wt.% PNIPAAM-co-MA decreased the ζ-potential absolute value meaning that the repulsions between INTs were reduced. According to the DLVO theory,[60] aggregation processes between imogolite nanotubes can be expected by reducing their repulsion forces. Moreover, the selective adsorption of PNIPAAM-co-MA onto the external surface of imogolite can favor INTs clustering because of hydrophobic interactions between the alkyl chains of the copolymer. The enhancement of the hydrodynamic radius is consistent with the formation of INTs clusters induced by PNIPAAM-co-MA. Similar observations were detected for halloysite nanotubes functionalized with PNIPAAM-NH_2 on their outer surface.[48] Figure 1C shows the dependence of the average hydrodynamic radius for INTs/PNIPAAM-co-MA with variable copolymer concentrations. For 0.1 wt.% PNIPAAM-co-MA, the average hydrodynamic radius was enhanced by ca. 45 nm in comparison with pristine imogolite (from ≈35 to 90 nm). A further copolymer addition reduced the average hydrodynamic radius of INTs/PNIPAAM-co-MA indicating that the aggregation between imogolite nanotubes is prevented. This finding agrees with the increase of the repulsions predicted by ζ-potential data (Figure 1A). Both ζ-potential and DLS results suggest that the addition of PNIPAAM-co-MA at 0.1 wt.% can favor the sedimentation of imogolite nanotubes dispersed in water, while this effect is disadvantaged by increasing the copolymer concentration. This hypothesis was supported by optical images of INTs/PNIPAAM-co-MA aqueous mixtures (**Figure 2B**). The mixing of imogolite with 0.1 wt.% copolymer destabilizes the clay nanotubes dispersed in water as evidenced by the formation of a clear sediment after 48 h from the preparation of the mixtures due to the INTs clustering. On the other hand, the mixtures containing larger PNIPAAM-co-MA amounts did not show any phase separation in agreement with their higher colloidal stability. It should be noted that aqueous dispersion of pristine imogolite nanotubes (Figure 2A) is stable up to several years.

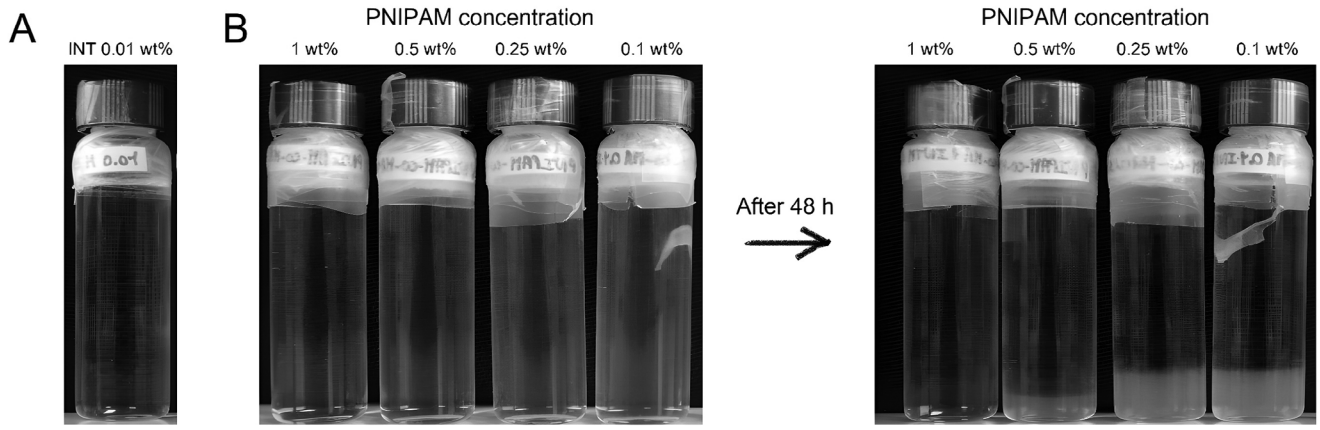

Figure 2. Influence of PNIPAAM-co-MA addition on the aqueous colloidal stability of imogolite nanotubes. A) Optical image of 0.01 wt.% INT aqueous suspension. B) Optical images of INTs/PNIPAAM-co-MA aqueous mixtures with variable copolymer content (from 0.1 to 1 wt.%) and constant concentration of imogolite (0.01 wt.%). The effect of the time (48 h from the preparation of the mixtures) is presented.

2.1.2. Effects of PNIPAAM-co-MA on the Structural Organization of Imogolite Nanotubes

We investigated the effects of PNIPAAM-co-MA addition on the organization of imogolite nanotubes dispersed in water by macroscopic optical observations between crossed polarizers and Small-angle X-ray scattering (SAXS) experiments. As shown in **Figure** 3A, 0.01 wt.% imogolite suspensions did not exhibit any birefringence indicating that the clay nanotubes are randomly dispersed in water. The addition of PNIPAAM-co-MA did not confer any ordering to the organization of imogolite nanotubes. In contrast, INT aqueous dispersion at higher concentration (0.1 wt.%) evidenced flow birefringence highlighting pretransitional effects toward a liquid-crystalline phase,[39] which is partially observed also by adding 0.1 wt.% PNIPAAM-co-MA (Figure 3B). On the other hand, the presence of 1 wt.% PNIPAAM-co-MA induced a complete destabilization of the nematic phase suggesting that the copolymer adsorption onto the imogolite surface generates a dealignment of the nanotubes.

SAXS data confirmed the observations determined by naked-eyed inspections of the samples between crossed polarizers. As shown in Supporting Information (Figure S2, Supporting Information), SAXS curves of 0.01 wt.% INTs dispersions (before and after the addition of PNIPAAM-co-MA) did not present any characteristic signals related to the presence of nematic phase. On the contrary, **Figure** 4 shows that the SAXS curve of 0.1 wt.% INT suspension evidenced a broad correlation peak at Q = 0.00595 $Å^{-1}$ corresponding to an average intertube distance $d = 2\pi/Q$ of ≈105.6 nm. The addition of 0.1 wt.% PNIPAAM-co-MA shifted the correlation peak to a lower Q-value of 0.00555 $Å^{-1}$ (d = 113 nm). This increase in the average intertube distance can be attributed to the interaction of the polymer with the outer surface of INTs. At 1 wt.% PNIPAAM-co-MA, the correlation peak related to the short-range positional order of the nanotubes completely vanished, but the scattered intensity still preserved a Q^{-1} dependence, indicating the lack of nanotube aggregation in this Q-range. Moreover, the first oscillation at high Q-value corresponding to the first minimum of the nanotube form

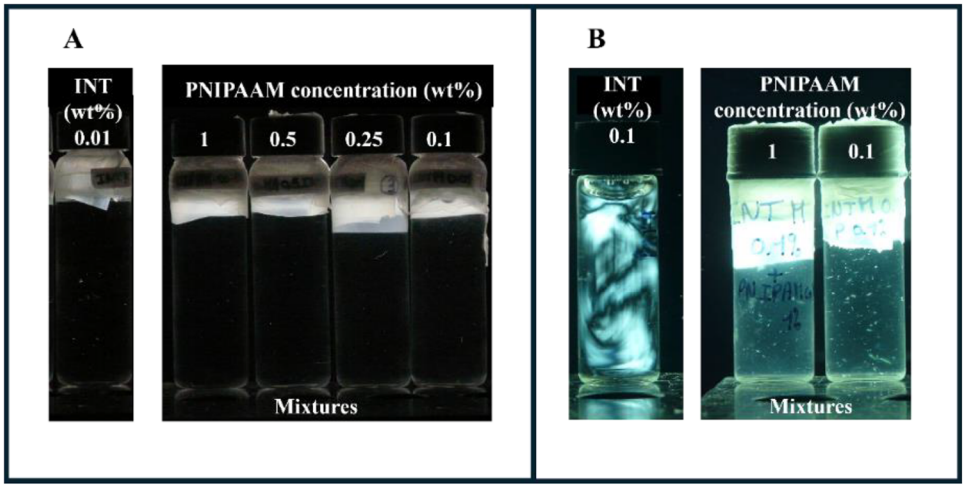

Figure 3. Optical observations between crossed polarizers of INT aqueous dispersions and INT/PNIPAAM-co-MA mixtures in water prepared with different imogolite concentrations. A) 0.01 wt.%. B) 0.1 wt.%.

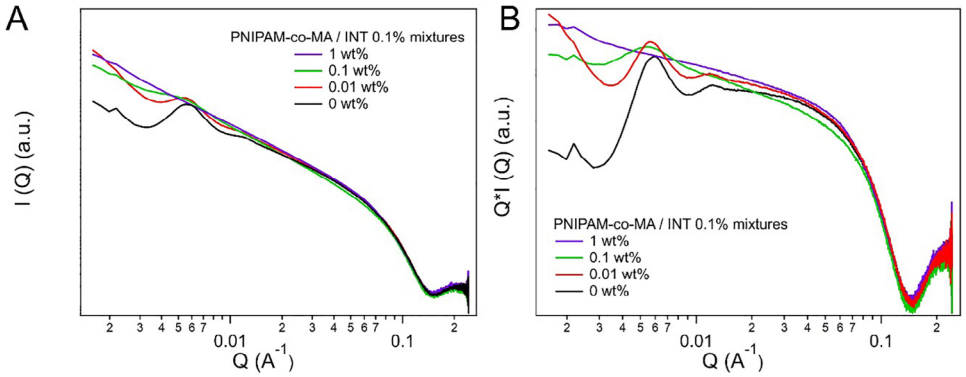

Figure 4. SAXS curves of PNIPAAM-co-MA/INTs mixtures at 25 °C. The polymer concentrations was changed from 0.01 to 1 wt.%, while the INTs concentration was kept constant at 0.1 wt.%. The small bump around Q ≈0.0025 $Å^{-1}$ is due to parasitic scattering close to the beamstop.

factor remains unchanged, indicating no alteration in the mean nanotube radii of INTs. Besides, I(Q) versus Q trends, Figure 4 shows Q.I(Q) versus Q plots for a better description of the SAXS profiles.

2.2. Thermo-Responsive Characteristics of Imogolite/PNIPAAM-co-MA Mixtures

2.2.1. Effect of Temperature on the Aqueous Diffusion of Imogolite/PNIPAAM-co-MA

DLS experiments were carried out as a function of temperature to investigate the thermo-responsive characteristics of imogolite clay nanotubes after PNIPAAM-co-MA adsorption. As shown in **Figure 5**A, the hydrodynamic diameter of pristine imogolite is constant at ≈40 nm highlighting that the aqueous dynamic behavior of clay nanotubes is not affected by temperature variations. On the other hand, Figure 5B–D compares the hydrodynamic diameter versus Temperature trends for PNIPAAM-co-MA dispersions and INTs/PNIPAAM-co-MA mixtures in water.

As a general result, we observed that both pristine PNIPAAM-co-MA and imogolite/PNIPAAM-co-MA hybrids present a sharp increase in the hydrodynamic diameter that is attributed to the formation of aggregates induced by dehydration process of copolymers. In particular, dehydration of PNIPAAM-co-MA moieties can favor hydrophobic attractions between polymeric chains and the consequent coil-to-globule transition.[65,66] The transition temperature is defined as lower crystalline solution temperature (LCST). As a general result, we detected that the adsorption onto imogolite determine LCST decreases. This finding was confirmed by turbidimetric experiments through UV–vis spectroscopy (see Figure S3, Supporting Information). The interactions with imogolite surface reduced the clouding temperature of PNIPAAM-co-MA within a range between 30 and 35 °C. Similar observations were detected for PNIPAAM-NH_2 adsorbed onto the external surface of halloysite clay nanotubes.[48] It is noteworthy to evidence that the presence of the coil-to-globule transition in the imogolite/PNIPAAM-co-MA mixtures is consistent with the selective adsorption of copolymer onto the outer surface of INTs. According to this consideration, it is reported that LCST cannot be determine from DLS experiments on PNIPAAM-co-MA confined within the cavity of halloysite clay nanotubes.[48] It should be noted that the hydrodynamic diameters after LCST of INTs/PNIPAAM-co-MA are constant at ≈4000 nm, which is significantly larger with respect to the hydrodynamic diameters (≈100 nm) of pristine PNIPAAM-co-MA. Based on these results, we can exclude that PNIPAAM-co-MA is desorbed from imogolite surface during the temperature ramp.

2.2.2. Effects of Temperature on the Thermodynamic Properties of Imogolite/PNIPAAM-co-MA

The influence of imogolite on the specific volume (v_{sp}) and isoentropic compressibility (k_{sp}) of PNIPAAM-co-MA was investigated by densitometry and speed of sound experiments performed at variable temperatures (from 15 to 40 °C). As depicted in **Figure 6**, both parameters increase with the temperature in agreement with the positive expansibility of the copolymer.

In detail, the evolution of the specific volume on temperature sharply changed in correspondence to LCST due to the release of the water molecules from PNIPAAM-co-MA. In the first region (T < LCST), the slope of increasing trend is smaller because the copolymer is highly hydrated, and hydrogen bonds are predominant. Below LCST, the imogolite addition did not alter the slope of the v_{sp} versus T trend. On the other hand, the presence of INTs induced an increase in the slope within the second region (T > LCST) highlighting that imogolite favors the dehydration process. Accordingly, we observed that the fraction of free water molecules is slightly larger for INT/PNIPAAM-co-MA with respect to that of PNIPAAM-co-MA within the temperature range between 33 and 40 °C. Opposite results were detected in the interval between 15 and 32 °C (see Figure S4, Supporting Information).

As concerns the isoentropic compressibility values, we detected a monotonic increase with the temperature for pristine PNIPAAM-co-MA, while a step change at ≈33 °C was observed for INTs/PNIPAAM-co-MA. The negative k_{sp} values (determined up to ≈30 °C) are consistent with the coil conformation of the hydrated copolymer. On the other hand, we detected positive isoentropic compressibility at higher temperature in agreement with the formation of stable hydrophobic aggregates.[67] As shown in (Figure S5, Supporting Information), both specific volume and

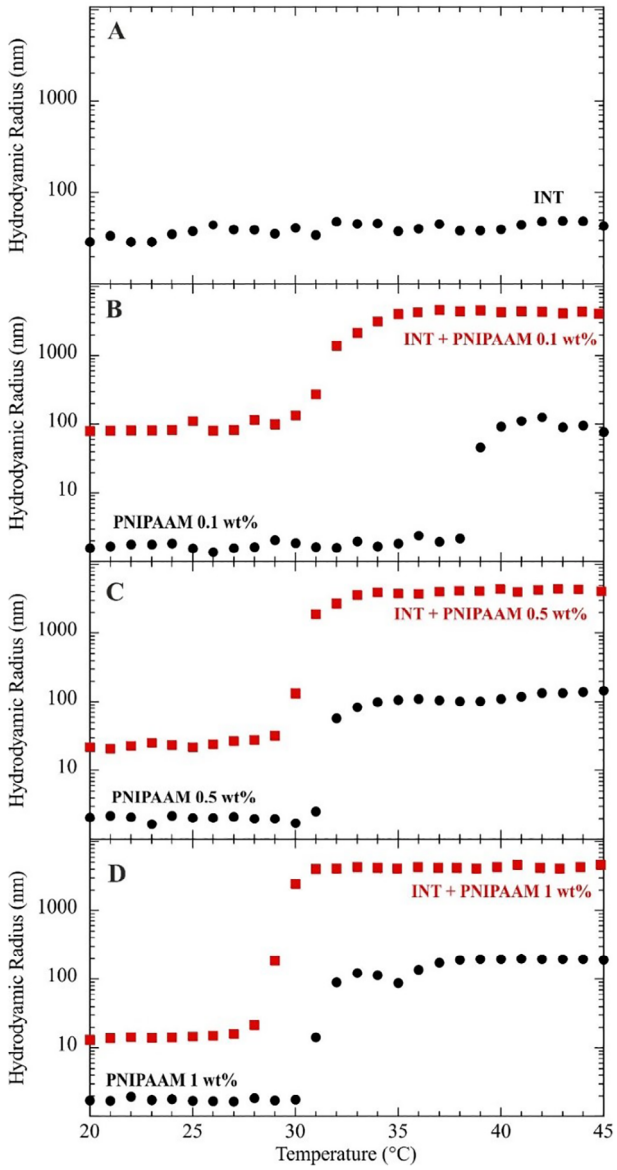

Figure 5. Effect of temperature on the aqueous diffusion of imogolite, PNIPAAN-co-MA and imogolite/PNIPAAM-co-MA dispersions. A) Dependence of hydrodynamic radius on temperature for 0.01 wt.% imogolite dispersion. B–D) Dependence of hydrodynamic radius on temperature for PNIPAAM-co-MA dispersion and imogolite/PNIPAAM-co-MA mixture. The copolymer concentration is variable (from 0.1 to 1 wt.%), while the content of imogolite is fixed at 0.01 wt.%.

isoentropic compressibility of imogolite nanotubes are not influenced by temperature variations.

2.2.3. Influence of Imogolite on the Thermodynamics of PNIPAAM-co-MA Phase Transition

Figure 7 shows the Differential Scanning Calorimetry (DSC) curves of PNIPAAM-co-MA and imogolite/PNIPAAM-co-MA dispersions obtained under heating and cooling ramps.

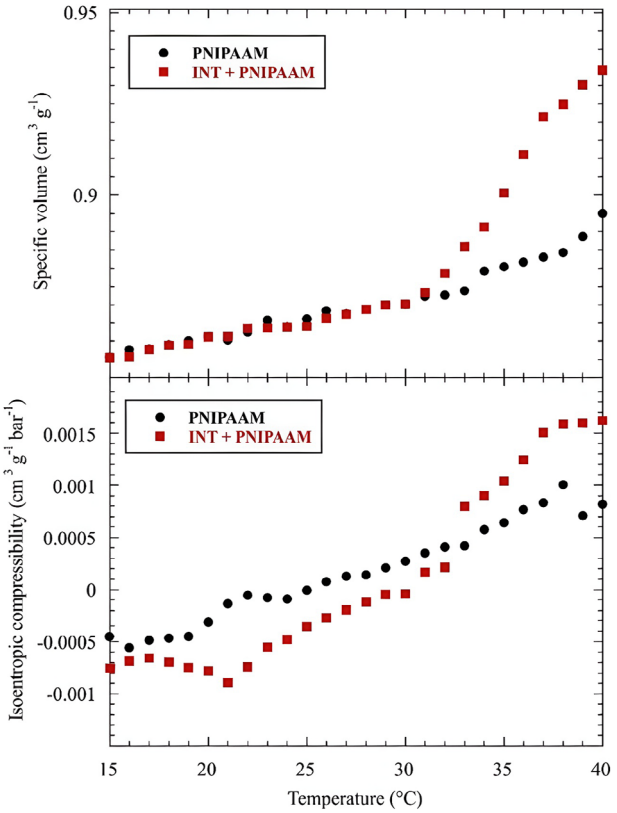

Figure 6. Density and Speed of sound experiments on PNIPAAM-co-MA and imogolite/PNIPAAM-co-MA dispersions. Effects of temperature on the specific volume (top) and isoentropic compressibility (bottom) of PNIPAAM-co-MA. The concentrations of PNIPAAM-co-MA and imogolite were set at 0.1 and 0.01 wt.%, respectively.

Both DSC thermograms during heating evidenced an endothermic signal that is related to the PNIPAAM-co-MA dehydration and the consequent coil-to-globule transition of the copolymer.[48] As reported elsewhere,[48,68] we determined the LCST values at the minimum of the endothermic peaks. We detected that the presence of imogolite induces a slight reduction of LCST from 35.1 to 33.8 °C. These results agree with the DLS trends (Figure 5) confirming that the imogolite addition decreases the LCST of PNIPAAM-co-MA. The integration of the DSC peaks allowed us to estimate the enthalpy variation (ΔH_d) due to the copolymer dehydration. We observed that the copolymer adsorption onto imogolite generates a significant ΔH_d reduction from 331 ± 11 to 185 ± 6 kJ mol^{-1}. This effect could indicate that PNIPAAM-co-MA moieties are partially dehydrated before LCST because of the electrostatic interactions between copolymer and imogolite. Moreover, imogolite nanotubes coated by PNIPAAM-co-MA can act as nucleating agents, favoring the aggregation of copolymer even before LCST. Similar results were detected for PNIPAAM adsorbed on halloysite nanotubes.[48]

DSC curves under cooling ramp (Figure 7) evidenced exothermic peaks that can be attributed to PNIPAAM-co-MA hydration highlighting that the coil-to-globule transition of the copolymer is a reversible process. The addition of imogolite shifted the exothermic signal to a lower temperature range.

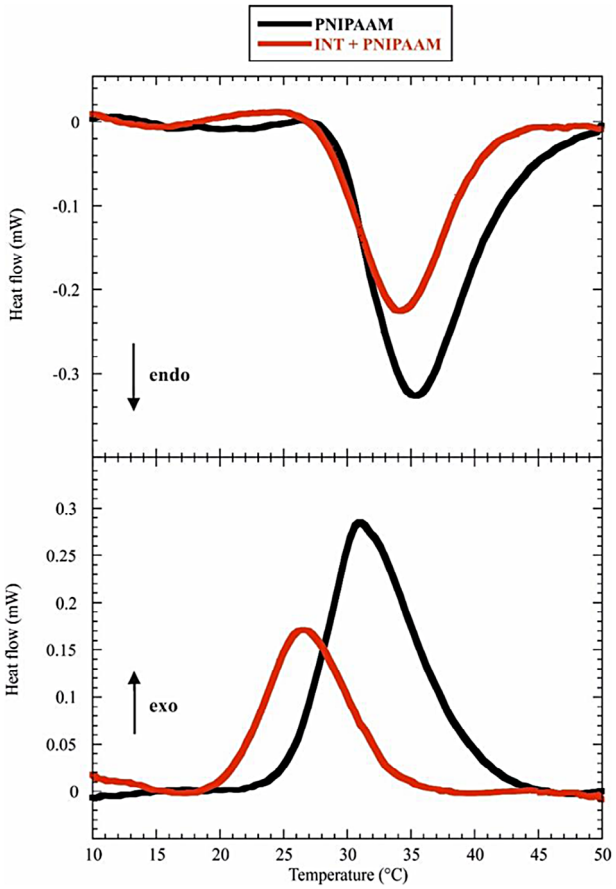

Figure 7. Differential Scanning calorimetry of PNIPAAM-co-MA and imogolite/PNIPAAM-co-MA dispersions. DSC curves under heating (top) and cooling (bottom) ramps. The concentrations of PNIPAAM-co-MA and imogolite were set at 1 and 0.01 wt.%, respectively.

Specifically, we determined that the temperatures at the maximum of DSC peaks are 30.8 and 26.4 °C for PNIPAAM-co-MA and imogolite/PNIPAAM-co-MA, respectively. As expected, the enthalpy changes (ΔH_H) for copolymer hydration are negative for both systems. The mixing with imogolite decreased the ΔH_H absolute value indicating that the heat released from globule-to-coil transition is reduced by PNIPAAM-co-MA adsorption onto INTs surface. We calculated ΔH_H values of -260 ± 9 and -142 ± 5 kJ mol^{-1} for PNIPAAM-co-MA and imogolite/PNIPAAM-co-MA, respectively.

2.2.4. Effects of Temperature on the Structural Organization of Imogolite/PNIPAAM-co-MA

Figure 8A presents the optical observations of INT dispersion and imogolite/PNIPAAM-co-MA mixtures kept at 45 °C. After the heating process (1 h at 45 °C), we do not observe as much birefringence of the INT suspension, meaning that the heating process seems to destabilize the nematic phase. Similarly, INT/PNIPAM-co-MA mixtures did not exhibit any birefringence, which implies the random organization of imogolite nanotubes in such conditions. However, we observed a turbid white colloid for the highest concentration of PNIPAM-co-MA (1% wt), which is related to

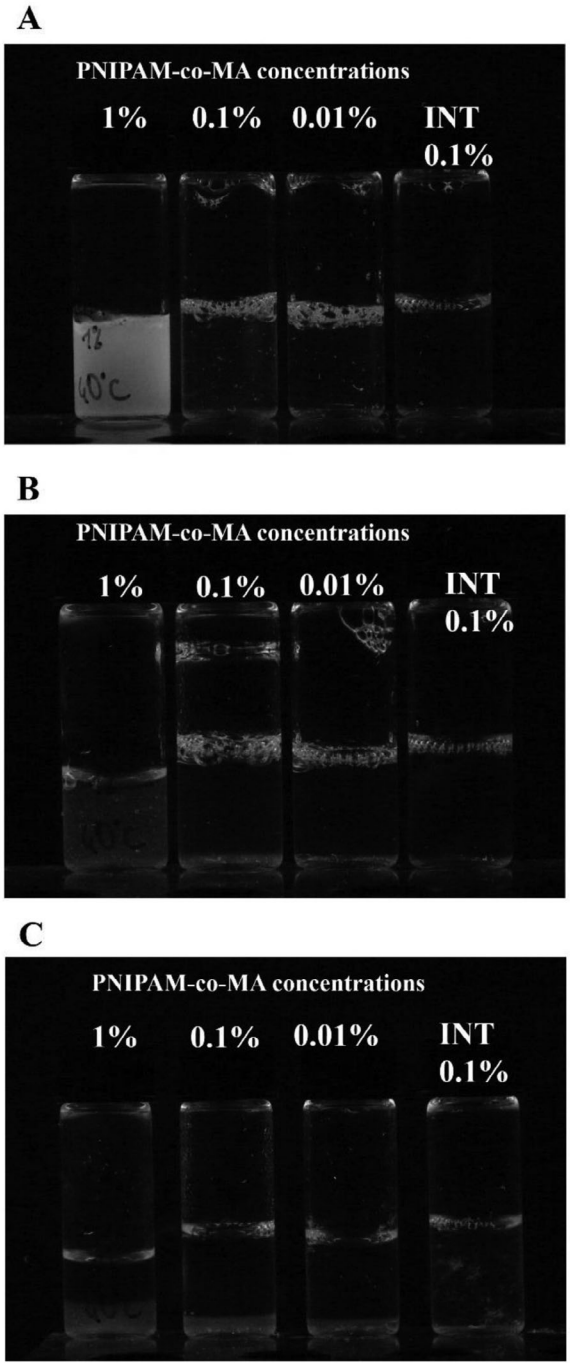

Figure 8. Macroscopic polarized optical observations of INT aqueous dispersions and INT/PNIPAAM-co-MA mixtures in water after their heating at 45 °C. A) POM images of the colloidal systems kept at 45 °C for 1 h, B) after return at 25 °C for 1 h, and C) after return at 25 °C for 48 h.

the coil-to-globule transition of the copolymer. Observations after the cooling of the suspensions from 45 to 25 °C and the subsequent stabilization for 1 h are presented in Figure 8B. Whatever the concentration of PNIPAM, the dispersions are all isotropic, and no preferential organization of the nanotubes is observed. Obviously, the mixture with 1 wt.% PNIPAM-co-MA is now

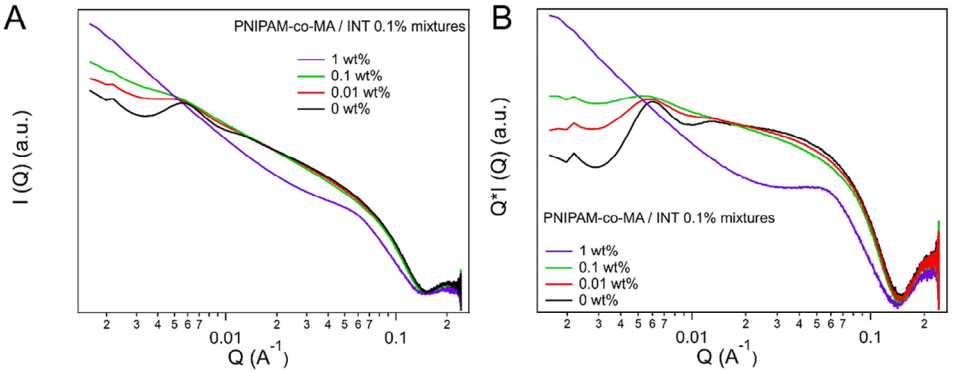

Figure 9. SAXS curves of PNIPAAM-co-MA/INTs after the heating process at 45 °C and their cooling to 25 °C for 48 h. The polymer concentrations were changed from 0.01 to 1 wt.%, while the INTs concentration was kept constant at 0.1 wt.%.

transparent due to the reversibility of the coil-to-globule transition of the copolymer. Furthermore, we performed observations 48 h after stabilizing at 25 °C (Figure 8C). We observed that PNIPAM-co-MA/INT mixtures present only a white precipitate at the bottom of the flask.

Besides these optical observations, we performed SAXS experiments on the suspensions after their heating/cooling cycle and the final stabilization at 25 °C for 48 h (**Figure 9**). We detected a broadening of the nematic peak between PNIPAAM-co-MA concentrations of 0 and 0.1 wt.% with a slight shift in the Q-value of the peak (0.00595 $Å^{-1}$ at 0 wt.% (105.6 nm, 0.174%), 0.00585 $Å^{-1}$ (107.4 nm, 0.168%) at 0.01 wt.% and 0.00575 $Å^{-1}$ (109.3 nm, 0.162%) at 0.1 wt.%). This shift can be attributed to the increase of the uncertainty in the determination of the peak due to its broadening. At PNIPAAM-co-MA 1 wt.%, the peak has completely disappeared but there is the appearance of a shoulder at 0.056 $Å^{-1}$ follow by a $I \approx Q^{-3.5}$ decrease. Also, the first oscillation at high Q-value corresponding to the nanotube form factor is slightly modified. This might be consistent with the formation of a network.

Furthermore, we investigated the thermodynamic and structural properties of INTs/PNIPAAM-co-MA at variable temperatures. The results revealed that the interactions with imogolite surfaces strongly affect the coil-to-globule transition of PNIPAAM-co-MA. The lower crystalline solution temperature (LCST) of the copolymer was reduced by the presence of imogolite, which also induced a relevant decrease in the enthalpy variation of the coil-to-globule transition. This effect could indicate that PNIPAAM-co-MA moieties are partially dehydrated before LCST due to the electrostatic attractions between the copolymer and imogolite. Structural investigations of the mixtures were conducted after heating/cooling cycle between 25 and 45 °C to explore the influence of temperature on the organization of imogolite nanotubes. The results evidenced that temperature variations within the coil-to-globule transition do not prevent the destabilization effects of PNIPAAM-co-MA toward the INTs ordering. The attained knowledge represents a starting point for designing thermo-sensitive nanotubes suitable as drug delivery systems under variable physiological conditions, smart windows, and soft actuators.

3. Conclusion

In this paper, we studied the formation of supramolecular complexes obtained by electrostatic interactions between imogolite clay nanotubes (INTs) and Poly(*N*-isopropylacrylamide-co-methacrylic acid) (PNIPAAM-co-MA) dispersed in aqueous medium. As expected, anionic PNIPAAM-co-MA was selectively adsorbed onto the INTs outer surface, which is positively charged. Accordingly, the adsorption of the copolymer induced an inversion of the positive surface charge of imogolite as well as a reduction of the aqueous dynamic behavior of imogolite nanotubes depending on the PNIPAAM-co-MA concentration. Aggregation processes were detected for aqueous mixtures of INTs (0.01 wt.%) and PNIPAAM-co-MA (0.1 wt.%). The increase of PNIPAAM-co-MA concentration prevented the clustering between INTs, enhancing the colloidal stability of the aqueous dispersions. According to SAXS and POM experiments, the adsorption of PNIPAAM-co-MA reduced the ordering of imogolite nanotubes in water, destabilizing the nematic phase.

4. Experimental Section

Preparation of Imogolite Nanotubes Dispersed in Water: Typically, a mixture of aluminum perchlorate (ACS reagent, ≥98%), urea (ACS reagent, 99%) and germanium (IV) ethoxide were mixed under stirring in a PFTE beaker to obtain a molar ratio [Ge]:[Al]:[urea] = 1:2:2, the initial aluminum perchlorate concentration being set at C = 0.2 mol L^{-1}. After homogenization, the beaker was transferred into an acid digestion bomb (Zeoclave, Maximator, France) that was placed in an oven (Memmert) at 140 °C for 5 days. After this ageing period, the autoclave was cooled down and the resulting suspension was placed in semi-permeable membranes (Spectra/Por, 10 kDa) to perform dialysis against ultrapure water until the conductivity of the dialysis bath was below 5 µS cm^{-1}. The concentration of the purified dispersion was realized by weight loss upon drying. Characterization of the structure of as-synthesized INTs was performed by transmission electron microscopy on a JEOL 1400 microscope operating at 80 kV. Infrared spectroscopy was carried out on a Nicolet iS50 spectrometer in transmission mode (4 cm^{-1} of resolution) with a KBr beamsplitter and a DTGS/KBr detector.

Preparation of Imogolite/PNIPAAM-co-MA Aqueous Mixtures: Imogolite dispersion (1 wt.%) was diluted with water by factors 1/10 and 1/100 to reduce the INT concentrations to 0.1 and 0.01 wt.%, respectively. Then, variable amounts of PNIPAM-co-MA were added to the diluted INT

dispersions to systematically change the INT/PNIPAM-co-MA mass ratio of the mixtures. INT/PNIPAM-co-MA mixtures were subjected to ultrasonication for 10 min and then magnetically stirred for 60 min. The temperature was kept at 25 °C. For comparison, PNIPAM-co-MA dispersions were prepared in water using the same protocol.

Characterization of the Dispersions: Dynamic light scattering (DLS) and ζ-potential experiments were carried out by means of a Zetasizer NANO-ZS (Malvern Instruments). ζ-potential tests were conducted at 25 °C using a disposable folded capillary cell, while DLS measurements were performed in isothermal conditions (T = 25 °C) as well as under a heating ramp from 20 to 45 °C. The wavelength and the scattering angle were fixed at 632.8 nm and 173°, respectively.

The specific volume and the isoentropic compressibility were determined by density and speed of sound measurements conducted at variable temperatures (from 15 to 40 °C) by using DSA 5000 M (Anton Paar) apparatus. The combination of density and speed of sound data allowed them to estimate the fraction of free water molecules.

Turbidimetric experiments were conducted by UV–vis spectroscopy using a Specord S600 Analytik Jena instrument. The measurements were conducted at variable temperatures (from 20 to 45 °C).

The thermodynamics of coil-to-globule transition of PNIPAAM-co-MA was studied by micro differential scanning calorimetry (micro-DSC) analysis. These experiments were performed by using a Setaram DSC III apparatus under constant nitrogen flow in the range from 10 to 50 °C. Both heating and cooling ramps were carried out with a scan rate of 1 °C min^{-1}. The stainless steel (1 cm^3) sample cell was filled with ≈500 mg of the aqueous dispersion, and the reference cell with the corresponding amount of water. The calibration was performed by using naphthalene.

Macroscopic polarized optical observations were realized between crossed polarizers in a home-made setup equipped with a Panasonic DMC-FZ18camera. The aqueous dispersions were transferred to 12 cm^3 glass vials and stored vertically prior to observations.

Small-angle X-ray scattering experiments were carried out at the SWING beamline of SOLEIL synchrotron (Saint-Aubin, France). The incident wavelength was fixed at $\lambda = 1.0332$ Å. SAXS patterns were acquired on a 2D detector (Eiger 4 M, Dectris Ltd., Switzerland) placed in a vacuum tunnel at a distance of ≈6 m from the sample. In this case, aqueous dispersions were transferred into cylindrical borosilicate glass capillaries (WJMGlas/Müller GmbH, DE) that were flame-sealed and stored vertically. Angular integration of the scattering patterns, giving the dependence of the scattered intensity as a function of the scattering vector modulus Q ($Q = 4\pi \sin(\theta) / \lambda$ with 2θ is the scattering angle), was processed by using the Foxtrot software available on the beamline.

Supporting Information

Supporting Information is available from the Wiley Online Library or from the author.

Acknowledgements

This work had benefited from an Investissements d'Avenir grant from Labex PALM (ANR-10-LABX-0039-PALM). C.H. and E.P. acknowledge SOLEIL synchrotron for the allocation of beamtime on the SWING beamline under the approved proposal BAG 20231786. The work was supported by the University of Palermo and the FFR 2025 project.

Conflict of Interest

The authors declare no conflict of interest.

Data Availability Statement

The data that support the findings of this study are available from the corresponding author upon reasonable request.

Keywords

composite, electrostatic attractions, Imogolite nanotubes, LCST, Poly (N-isopropylacrylamide-co-methacrylic acid)

Received: March 7, 2025
Revised: April 18, 2025
Published online:

[1] M. Liu, R. Fakhrullin, A. Stavitskaya, V. Vinokurov, N. Lama, Y. Lvov, *Sci. Technol. Adv. Mater.* **2024**, *25*, 2327276.
[2] Y. Feng, X. Chen, R.-R. He, Z. Liu, Y. M. Lvov, M. Liu, *ACS Nano* **2024**, *18*, 20001.
[3] Y. Feng, X. Luo, Z. Li, X. Fan, Y. Wang, R.-R. He, M. Liu, *Nat. Commun.* **2023**, *14*, 5083.
[4] P. Dramou, M. Fizir, A. Taleb, A. Itatahine, N. S. Dahiru, Y. A. Mehdi, L. Wei, J. Zhang, H. He, *Carbohydr. Polym.* **2018**, *197*, 117.
[5] A.-M. Milisav, L. Sotelo, C. Cantallops-Vilà, T. Fontanot, I. Erceg, K. Bojanić, T. Vuletić, Ž. Fiket, M. Ivanić, S. Christiansen, E. Meurice, M. D. Sikirić, *Adv. Mater. Interfaces* **2025**, *12*, 2400631.
[6] T. Tarhan, A. Dündar, V. Okumuş, M. Çulha, *ChemistrySelect* **2021**, *6*, 4217.
[7] K. Ariga, D. T. Leong, T. Mori, *Adv. Funct. Mater.* **2018**, *28*, 1702905.
[8] Y. Liu, H. Guan, J. Zhang, Y. Zhao, J.-H. Yang, B. Zhang, *Int. J. Hydrog. Energy* **2018**, *43*, 2754.
[9] M. Fahimizadeh, L. W. Wong, Z. Baifa, S. Sadjadi, S. A. B. Auckloo, K. Palaniandy, P. Pasbakhsh, J. B. L. Tan, R. K. R. Singh, P. Yuan, *Appl. Clay Sci.* **2024**, *251*, 107319.
[10] M. alleshagh, S. Sadjadi, H. Arabi, N. Bahri-Laleh, E. Monflier, *Mater. Chem. Phys.* **2022**, *278*, 125506.
[11] M. Fizir, A. Richa, S. Touil, Y. Benmokadem, K. Boubekeur, B. Hallal, H. Drici, L. Wei, *Environ. Prog. Sustain. Energy* **2023**, *42*, 13995.
[12] S. Lotito, D. Cignolo, J. Gubitosa, G. Barucca, P. Mengucci, M. Striccoli, F. Palumbo, P. Cosma, P. Fini, S. Murgolo, V. Rizzi, F. Fracassi, A. Milella, A. Perrotta, *Adv. Mater. Interfaces* **2024**, *12*, 2400831.
[13] M. R. Caruso, M. M. Calvino, P. Šiler, L. Cába, S. Milioto, L. Lisuzzo, G. Lazzara, G. Cavallaro, *Small* **2025**, *21*, 2405215.
[14] O. Owoseni, Y. Su, S. Raghavan, A. Bose, V. T. John, *J. Colloid Interface Sci.* **2022**, *620*, 135.
[15] E. Boccalon, P. Sassi, L. Pioppi, A. Ricci, M. Marinozzi, G. Gorrasi, M. Nocchetti, *Appl. Clay Sci.* **2022**, *227*, 106592.
[16] E. Boccalon, G. Viscusi, A. Sorrentino, F. Marmottini, M. Nocchetti, G. Gorrasi, *Colloids Surf. Physicochem. Eng. Asp.* **2021**, *627*, 127135.
[17] J. J. Andrew, H. N. Dhakal, *Compos. Part C Open Access* **2022**, *7*, 100220.
[18] N. Gray-Wannell, P. Cubillas, Z. Aslam, P. J. Holliman, H. C. Greenwell, R. Brydson, E. Delbos, L.-J. Strachan, M. Fuller, S. Hillier, *Clay Miner.* **2023**, *58*, 395.
[19] E. Rozhina, S. Batasheva, R. Miftakhova, X. Yan, A. Vikulina, D. Volodkin, R. Fakhrullin, *Appl. Clay Sci.* **2021**, *205*, 106041.
[20] A. Lo Bianco, M. M. Calvino, G. Cavallaro, L. Lisuzzo, P. Pasbakhsh, S. Milioto, G. Lazzara, Y. Lvov, *Small* **2024**, *20*, 2406812.
[21] Y. Zhao, S. Guo, X. Xue, C. Xiong, X. Gao, B. Zhang, *Chem. Eng. J.* **2024**, *483*, 149332.
[22] W. Ma, W. O. Yah, H. Otsuka, A. Takahara, *J. Mater. Chem.* **2012**, *22*, 11887.
[23] M. Emanet, E. Kazanç, Z. Çobandede, M. Çulha, *Carbohydr. Polym.* **2016**, *151*, 313.
[24] K. Ariga, *Adv. Phys. Res.* **2023**, *2*, 2200113.
[25] Y. Wang, X. Ba, B. Zhang, Y. Wang, Y. Wu, H. Zhang, *J. Colloid Interface Sci.* **2024**, *657*, 344.

[26] A. Vikulina, D. Voronin, R. Fakhrullin, V. Vinokurov, D. Volodkin, *New J. Chem.* **2020**, *44*, 5638.
[27] N. Rahman, F. H. Scott, Y. Lvov, A. Stavitskaya, F. Akhatova, S. Konnova, G. Fakhrullina, R. Fakhrullin, *Pharmaceutics* **2021**, *13*, 1477.
[28] Y. Lvov, W. Wang, L. Zhang, R. Fakhrullin, *Adv. Mater.* **2016**, *28*, 1227.
[29] E. Paineau, *Appl. Sci.* **2018**, *8*, 1921.
[30] E. Puel, C. C. D. Coumes, A. Poulesquen, F. Testard, A. Thill, *J. Colloid Interface Sci.* **2023**, *647*, 478.
[31] Y. Higaki, A. Takahara, *Polym. J.* **2022**, *54*, 473.
[32] K. Shikinaka, *Polym. J.* **2016**, *48*, 689.
[33] V. D. Samith, S. Navarro, R. Dabirian, *ACS Omega* **2020**, *5*, 20707.
[34] P. Picot, F. Gobeaux, T. Charpentier, L. Belloni, A. Takahara, S.-I. Wada, A. Thill, *Appl. Clay Sci.* **2024**, *258*, 107497.
[35] E. Paineau, S. Rouzière, G. Monet, C. C. Diogo, I. Morfin, P. Launois, *J. Colloid Interface Sci.* **2020**, *580*, 275.
[36] E. Paineau, G. Monet, V. Peyre, C. Goldmann, S. Rouzière, P. Launois, *Langmuir* **2019**, *35*, 12451.
[37] C. Hotton, T. Bizien, B. Pansu, C. Hamon, E. Paineau, *Adv. Mater. Interfaces* **2024**, *11*, 2400323.
[38] K. Shikinaka, K. Shigehara, *Colloids Surf. Physicochem. Eng. Asp.* **2015**, *482*, 87.
[39] E. Paineau, M.-E. M. Krapf, M.-S. Amara, N. V. Matskova, I. Dozov, S. Rouzière, A. Thill, P. Launois, P. Davidson, *Nat. Commun.* **2016**, *7*, 10271.
[40] N. Arancibia-Miranda, M. Escudey, M. Molina, M. T. García-González, *J. Non-Cryst. Solids* **2011**, *357*, 1750.
[41] N. Jiravanichanun, K. Yamamoto, K. Kato, J. Kim, S. Horiuchi, W.-O. Yah, H. Otsuka, A. Takahara, *Biomacromolecules* **2012**, *13*, 276.
[42] L. Li, A. Takada, W. Ma, S. Fujikawa, M. Ariyoshi, K. Igata, M. Okajima, T. Kaneko, A. Takahara, *Langmuir* **2020**, *36*, 1718.
[43] N. A. Shaibie, N. A. Ramli, N. D. F. Mohammad Faizal, T. Srichana, M. C. I. Mohd Amin, *Macromol. Chem. Phys.* **2023**, *224*, 2300157.
[44] Z. Jiang, Y. Chen, M. Xu, W. Shao, L. Zhang, C. Liu, *Adv. Mater. Interfaces* **2023**, *10*, 2202047.
[45] X.-Z. Zhang, D.-Q. Wu, C.-C. Chu, *Biomaterials* **2004**, *25*, 3793.
[46] M. L. Ohnsorg, J. M. Ting, S. D. Jones, S. Jung, F. S. Bates, T. M. Reineke, *Polym. Chem.* **2019**, *10*, 3469.
[47] S. Throat, S. Bhattacharya, *Adv. Polym. Technol.* **2024**, *2024*, 1444990.
[48] G. Cavallaro, G. Lazzara, L. Lisuzzo, S. Milioto, F. Parisi, *Nanotechnology* **2018**, *29*, 325702.
[49] P. Agnihotri, Sangeeta, S. A., A. Dan, *Soft Matter* **2021**, *17*, 9595.
[50] A. Das, A. Babu, S. Chakraborty, J. F. R. Van Guyse, R. Hoogenboom, S. Maji, *Adv. Funct. Mater.* **2024**, *34*, 2402432.
[51] G. Ju, J. Tang, Q. Cheng, C. Wang, R. Liang, G. Sun, *Polymer* **2024**, *308*, 127355.
[52] S. Pasban, H. Raissi, *Sci. Rep.* **2022**, *12*, 14363.
[53] K. Shikinaka, T. Yokoi, Y. Koizumi-Fujii, M. Shimotsuya, K. Shigehara, *RSC Adv.* **2015**, *5*, 46493.
[54] S. Das, D. Patra, S. Shankar, A. Ajayaghosh, *Angew. Chem., Int. Ed.* **2022**, *61*, 202207641.
[55] D. Patra, S. Das, S. Shankar, A. Ajayaghosh, *Adv. Funct. Mater.* **2024**, *34*, 2408014.
[56] N. Sahu, C. Guchhait, I. Mohanta, V. Suriyaa, B. Adhikari, *Angew. Chem., Int. Ed.* **2025**, *64*, 202417508.
[57] M. Liu, Y. Ishida, Y. Ebina, T. Sasaki, T. Aida, *Nat. Commun.* **2013**, *4*, 2029.
[58] Y. S. Kim, M. Liu, Y. Ishida, Y. Ebina, M. Osada, T. Sasaki, T. Hikima, M. Takata, T. Aida, *Nat. Mater.* **2015**, *14*, 1002.
[59] E. Paineau, F. Bourdelle, R. Bhandary, L. Truche, C. Lorgeoux, M. Bacia-Verloop, G. Monet, S. Rouzière, D. Vantelon, V. Briois, P. Launois, *Small* **2024**, *20*, 2308665.
[60] C. Hotton, L. L. Roux, C. Goldmann, S. Rouzière, P. Launois, T. Bizien, E. Paineau, *J. Colloid Interface Sci.* **2024**, *664*, 857.
[61] M. Mukai, A. Takada, A. Hamada, T. Kajiwara, A. Takahara, *RSC Adv.* **2021**, *11*, 31712.
[62] Y. Wang, T. Saito, S. Fakhreddine, S. Nagasaki, *Colloids Surf. Physicochem. Eng. Asp.* **2023**, *656*, 130444.
[63] E. Paineau, M. S. Amara, G. Monet, V. Peyre, S. Rouzière, P. Launois, *J. Phys. Chem. C* **2017**, *121*, 21740.
[64] M. Bonini, A. Gabbani, S. Del Buffa, F. Ridi, P. Baglioni, R. Bordes, K. Holmberg, *Langmuir* **2017**, *33*, 2411.
[65] L. Tavagnacco, E. Zaccarelli, E. Chiessi, *J. Mol. Liq.* **2020**, *297*, 111928.
[66] M. López-González, M. M. Rodrigo, M. Valiente, I. Trabado, F. Mendicuti, G. Marcelo, *Eur. Polym. J.* **2020**, *131*, 109695.
[67] G. Cavallaro, G. Lazzara, S. Milioto, F. Parisi, *J. Colloid Interface Sci.* **2016**, *461*, 346.
[68] G. Wang, P. Wu, *Soft Matter* **2016**, *12*, 925.